ACS APPLIED MATERIALS & INTERFACES

Research Article

www.acsami.org

Langmuir–Blodgett Films of Self-Assembled (Alkylether-Derivatized Zn Phthalocyanine)–(C_{60} Imidazole Adduct) Dyad with Controlled Intermolecular Distance for Photoelectrochemical Studies

Ievgen Obraztsov,[†] Krzysztof Noworyta,[†] Aaron Hart,[‡] Habtom B. Gobeze,[‡] Chandra B. KC,[‡] Wlodzimierz Kutner,[†,§,*] and Francis D'Souza[‡,*]

[†]Institute of Physical Chemistry, Polish Academy of Sciences, 44/52 Kasprzaka, 01-224 Warsaw, Poland

[‡]Department of Chemistry, University of North Texas, 1155 Union Circle, #305070, Denton, Texas 76203-5017, United States

[§]Faculty of Mathematics and Natural Sciences, School of Science, Cardinal Stefan Wyszynski University in Warsaw, Woycickiego 1/3, 01-938 Warsaw, Poland

Supporting Information

ABSTRACT: A multilayer Langmuir–Blodgett (LB) film of the self-assembled electron donor–acceptor dyad of Zn phthalocyanine, appended with four long-chain aliphatic ether peripheral substituents, and an imidazole adduct of C_{60} was prepared and applied as a photoactive material in a photoelectrochemical cell. Changes in the simultaneously recorded surface pressure and surface potential vs area per molecule compression isotherms for Langmuir films of the dyad and, separately, of its components helped to identify phase transitions and mutual interactions of molecules in films. The Brewster angle microscopy (BAM) imaging of the Langmuir films showed circular condensed phase domains of the dyad molecules. The determined area per molecule was lower than that estimated for the dyad and its components, separately. The multilayer LB films of the dyad were transferred onto hydrophobized fluorine-doped tin oxide-coated (FTO) glass slides under different conditions. The presence of both components in the dyad LB films was confirmed with the UV–vis spectroscopy measurements. For the LB films transferred at different surface pressures, the PM-IRRAS measurements revealed that the phthalocyanine macrocycle planes and ether moieties in films were tilted with respect to the FTO surface. The AFM imaging of the LB films indicated formation of relatively uniform dyad LB films. Then, the femtosecond transient absorption spectral studies evidenced photoinduced electron transfer in the LB film. The obtained transient signals corresponding to both $Zn(TPPE)^{\bullet+}$ and $C_{60}im^{\bullet-}$ confirmed the occurrence of intramolecular electron transfer. The determined rate constants of charge separation, $k_{cs} = 2.6 \times 10^{11}\ s^{-1}$, and charge recombination, $k_{cr} = 9.7 \times 10^{9}\ s^{-1}$, indicated quite efficient electron transfer within the film. In the photoelectrochemical studies, either photoanodic or photocathodic current was generated depending on the applied bias potential when the dyad LB film-coated FTO was used as the working electrode and ascorbic acid or methylviologen, respectively, as the charge mediator in an aqueous solution.

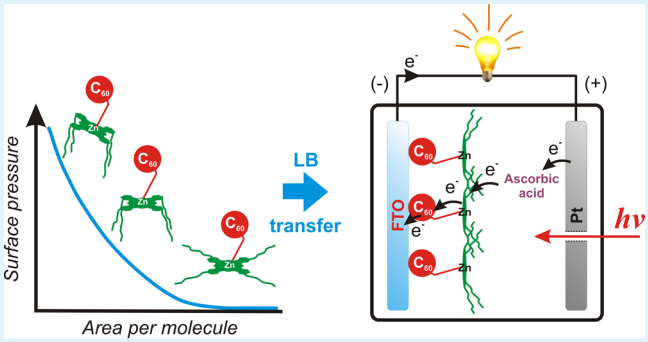

KEYWORDS: *zinc phthalocyanine, C_{60} fullerene, imidazole adduct of C_{60}, donor–acceptor dyad, photoelectrochemistry, supramolecular assembling, Langmuir–Blodgett film*

INTRODUCTION

To meet the ever-increasing global energy needs, research on the synthesis of photoelectroactive compounds and their subsequent use for building devices for light energy harvesting has seen a steady growth.[1−10] Toward this, researchers have extensively studied electron donor–acceptor dyads of metallophthalocyanines or metalloporphyrins and C_{60} adducts among others.[11−17]

There are two common approaches to form a (metallophthalocyanine or metalloporphyrin)–(C_{60} adduct) donor–acceptor dyad.[18−20] One uses covalent bonding that links both moieties together.[21] The other involves supramolecular self-assembling of the donor and acceptor molecules by virtue of H-bonding, electrostatic interactions,[22] metal–ligand coordination,[23−25] and π–π plane-to-plane stacking of their aromatic rings.[26−29] The latter self-assembly methods have has provided an opportunity to construct organized donor–acceptor dyads according to the bottom-up self-assembly approach to probe vectorial electron transfer when the dyads are surface immobilized.[30−33] Consequently, it has been possible to control

Received: March 13, 2014
Accepted: May 1, 2014
Published: May 1, 2014

Scheme 1. (a) Reaction Equations of the Tetrakis(2,9,16,23-[triethyleneglycolmonomethyl ether]-phthalocyaninato)Zn(II), Zn(TPPE), Synthesis; (b) Proposed Structural Formula of the Zn(TPEE)-C_{60}im Electron Donor−Acceptor Dyad Used for Preparation of the Langmuir and Langmuir−Blodgett Films; Tetrakis(2,9,16,23-[triethyleneglycolmonomethyl ether] phthalocyaninato) Zn(II), Zn(TPPE) 2, and [*N*-methyl-2-(4′-*N*-imidazolylphenyl)-3,4-fulleropyrrolidine], C_{60}im 3

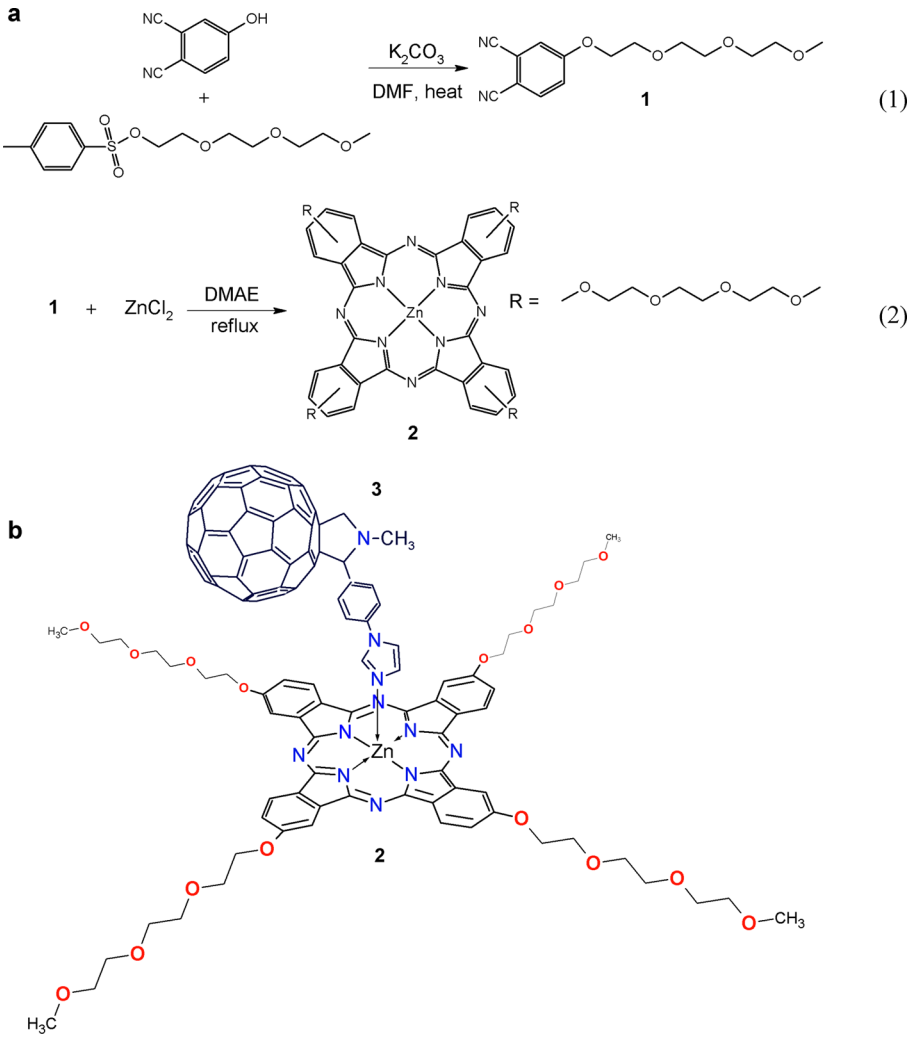

the direction of the electron flow in the light energy conversion devices constructed using these organized dyads by generating either anodic or cathodic photocurrents.[34−38]

As continuation of our efforts to devise organic photovoltaic materials by constructing organized donor−acceptor dyads on conducting transparent electrode surfaces and subsequent evaluation of their ability of light-to-electricity conversion,[39−41] in the present study we have utilized a zinc phthalocyanine as the electron donor and a fullerene derivative as the electron acceptor, and metal−ligand axial binding to connect them together. Using the LB technique, we have assembled on the FTO surface films of well-organized donor−acceptor pairs suitable for probing vectorial electron transfer, and characterized them by the electrochemical, BAM, AFM, and STM techniques. The photoinduced electron transfer in the donor−acceptor system studied has been established using the femtosecond pump−probe method. Further, the ability of these donor−acceptor films immobilized on electrodes to convert light into electricity and produce either cathodic or anodic photocurrents, depending upon the experimental conditions, has been evaluated by building photoelectrochemical devices.

EXPERIMENTAL SECTION

Chemicals and Materials. [C_{60}]Fullerene (+99.95%) for synthesis of the C_{60} imidazole adduct was from SES Research. All the reagents were from Aldrich Chemicals while the bulk solvents for the syntheses were from POCh or Fischer Chemicals. Optically transparent conducting FTO TEC 7 glass electrodes were from Pilkington North America, Inc. The highly oriented pyrolytic graphite (HOPG) was from Bruker. Water for the Langmuir film subphase was distilled and further purified (18.2 MΩ cm) with the Milli-Q filtering system of Millipore Corp., which was equipped with one carbon and two ion-exchange cartridge stages. All reagents were used as received. The imidazole adduct of C_{60} [*N*-methyl-2-(4′-*N*-imidazolylphenyl)-3,4-fulleropyrrolidine], C_{60}im, was synthesized according to the literature procedure,[42] whereas the herein developed two-step procedure of the tetrakis[2,9,16,23-tri(ethylene glycolmonomethyl ether) phthalocyaninato] Zn(II), Zn(TPPE) (Scheme 1a) is provided in the Supporting Information.

Instrumentation. The Langmuir films on the water subphase were prepared by using a computerized system of 601BAM trough (total area of 490 cm^2) of Nima Technology, Ltd. Surface pressure was measured with accuracy of ∼0.1 mN m^{-1} by using a PS4 sensor of Nima Technology of a Wilhelmy plate type. Surface potential was measured with accuracy of ∼10 mV by using an integrated Model 320C−H−CE noncontact voltmeter with the Model 3250 Kelvin

probe of Trek Inc. The multilayer LB films of the dyad were transferred onto different solid substrates with the D1L linear dipper of Nima Technology.

The UV−vis spectra were measured with the Model UV2501PC UV−vis recording spectrophotometer of Shimadzu. The ATR-FTIR spectra were recorded with the Vertex 80v FT-IR spectrophotometer equipped with the single-reflection diamond crystal Platinum ATR accessory of Bruker. For those measurements, a room temperature deuterated triglicine sulfate (DTGS) detector was used. The PM-IRRAS spectra, were recorded at 83° incidence angle with the same spectrophotometer, equipped with the PMA50 accessory, of Bruker. A nitrogen-cooled MCT detector of the accessory and ZnSe photoelastic modulator were used for that.

The electrochemical experiments were performed using the AUTOLAB pgstat 101 computerized electrochemistry system driven by the Nova software of Metrohm Autolab. A platinum disk and glass slides, coated with either the Au-over-Ti or FTO films, were used as the working electrodes. A platinum wire and an Ag/AgCl electrode served as the counter and reference electrode, respectively.

A Brewster angle microscope type EP3-BAM of NFT-Nanofilm Technologie, GmbH, was used for Brewster angle microscopy (BAM) imaging of Langmuir films spread on the water subphase. Tapping mode atomic force microscopy (AFM) and scanning tunneling microscopy (STM) imaging was performed with the NanoScope V microscope of Bruker using the NanoScope V8.15 software of the same manufacturer.

All the solutions were purged with argon prior to electrochemical measurements. Before film deposition, the FTO and Au-over-Ti coated glass slides were treated with the argon, Ar/O_2, or O_2 plasma using the model ZEPTO of Diener electronic GmbH plasma cleaner. All measurements were performed at ambient temperature, 25(±1) °C.

The DFT quantum-chemical calculations were performed on the workstation with four quad-core Xeon processors using Gaussian 09 rev C software[43] of Gaussian, Inc. The B3LYP functional along with the 3-21G* basis set, implemented in the software, were used for all the calculations.

Photoelectrochemical experiments were performed using the setup composed of the Oriel 6253 150 W xenon lamp with the AM1.5 filter, the shutter, and the pulse generator. The incident-photon-to-electron conversion efficiency (IPCE) was determined using the system composed of the 500-W Xe lamp set in an Oriel Instruments model 66021 housing and an Oriel Multispec 257 monochromator with a bandwidth of 4 nm. Absolute intensity of the incident light from the monochromator was controlled with an Optronic Laboratories Model 730A radiometer/photometer. Potential was controlled with the potentiostat/galvanostat Model 660D of CH Instruments.

Femtosecond transient absorption spectroscopy experiments were performed using an Ultrafast Femtosecond Laser Source (Libra) by Coherent incorporating diode-pumped, mode locked Ti:sapphire laser (Vitesse) and a diode-pumped intra cavity doubled Nd:YLF laser (Evolution) to generate a compressed laser output of 1.45 W. For optical detection, a Helios transient absorption spectrometer coupled with femtosecond harmonics generator, both provided by Ultrafast Systems LLC, was used. The source for the pump and probe pulses were derived from the fundamental output of Libra (Compressed output 1.45 W, pulse width 100 fs) at a repetition rate of 1 kHz. 95% of the fundamental output of the laser was introduced into harmonic generator, which generated the second and third harmonics of 400 and 267 nm beside the fundamental 800 nm for excitation, while the rest of the output was used for generation of white light continuum. In the present study, the second harmonic 400 nm excitation pump was used in all the experiments. Kinetic traces at appropriate wavelengths were assembled from the time-resolved spectral data. Data analysis was performed using the Surface Xplorer software of Ultrafast Systems.

Procedures. *Recording of Langmuir Compression Isotherms.* Before measurements, the surface of the water subphase was cleaned by repeated compressing, then aspirating traces of surface-active impurities and, subsequently, expanding. Surface pressure of the blank subphase solution was lower than 0.1 mN m^{-1} in the cleaning compression−expansion cycles. For Langmuir film preparation, chloroform solutions of 0.1 mM Zn(TPPE), C_{60}im, and the Zn(TPPE)-C_{60}im donor−acceptor dyad were prepared. Then, 150-μL solution sample of Zn(TPPE) or Zn(TPPE)-C_{60}im, or 350-μL solution sample of C_{60}im was evenly dispensed onto the water surface in consecutive experiments. Next, the chloroform solvent was allowed to evaporate for 15 min. Finally, isotherms of surface pressure (π) and surface potential (V) against area per molecule (A) were simultaneously recorded for the dyad and, separately, for its both components, under a compression regime at the rate of 25 cm^2 min^{-1}.

Langmuir−Blodgett Transferring of Langmuir Films. The best performing in photoelectrochemical experiments Langmuir films were transferred onto the substrates of HOPG plates as well as those of the hydrophobized with trimethoxyphenylsilane FTO glass slides and the 1-dodecanethiol hydrophobized Au-over-Ti film coated glass slides. For that, the Langmuir−Blodgett (LB) technique was used at surface pressure of 10 mN m^{-1} and the dipping linear rate of 5 mm min^{-1} (corresponding to the surface rate of 1.9 cm^2 min^{-1}). The transfer was initiated after the Langmuir film was kept for 15 min at the surface pressure characteristic for the transfer.

Other LB films of the dyad were transferred at the 10, 15, and 30 mm min^{-1} linear transfer rate (corresponding to the 3.8, 5.7, and 11.4 cm^2 min^{-1} surface rate) onto the FTO slides of different surface hydrophobicity at surface pressure of 8, 10, 15, or 24 mN m^{-1}. The substrate slides were rinsed with acetone, and then dried in an air stream, and/or plasma-cleaned under different conditions, or surface modified with trimethoxyphenylsilane prior to the LB experiments.

Surface Modification of Solid Substrates. The FTO glass slides were rinsed with acetone, dried, O_2-plasma cleaned, and activated, and then immersed in the 20 mM trimethoxyphenylsilane ethanol solution for 12 h. Finally, the slides were rinsed with ethanol, and then dried before use. The Au-over-Ti coated glass slides were rinsed with acetone, dried, Ar-plasma cleaned, and then immersed in 10 mM 1-dodecanethiol ethanol solution for 12 h. Finally, the slides were rinsed with ethanol, and then dried before use.

Brewster Angle Microscopy Imaging of the Langmuir Films. Changes of surface morphology of the Langmuir films were in situ BAM imaged, with 2-μm resolution, at surface pressure of 0, 1, and 10 mN m^{-1}. The first picture, i.e., that at zero surface pressure, was taken at 15 min after spreading the solutions of the compounds to allow for complete evaporation of the solvent.

Photoelectrochemical Experiments. The photoelectrochemical experiments were performed using a homemade PTFE cell featuring a quartz window. An FTO/[C_{60}im-Zn(TPPE) LB film], platinum plate, and an Ag/AgCl electrode served as the photoelectrode, counter electrode, and reference electrode, respectively. A 5 mm diameter area of the photoelectrode was exposed to light. A solution of 1 mM ascorbic acid in 0.1 M NaH_2PO_4 (pH = 4.1) or 5 mM methylviologen in 0.1 M Na_2SO_4 was used as the working solution in the photoelectrochemical experiments. The electrode was illuminated from the electrolyte/electrode interface side with light of 100 mW cm^{-2} intensity. The measurements of IPCE of conversion were performed under monochromatic light illumination.

RESULTS AND DISCUSSION

A simplified structure of the donor−acceptor dyad, composed of Zn(TPPE) **2** and C_{60}im **3**, is shown in Scheme 1b. The ether substituents of Zn(TPPE) played a triple role. First, they assured effective spreading of the dyad molecule on surface of the water subphase in the Langmuir film due to their hydrophilicity. This 2D stretch governed subsequent orientation of the dyad molecules in the LB film with respect to the FTO electrode substrate (see below). Second, these substituents helped keeping the phthalocyanine entities sufficiently far apart to avoid dyad aggregation. Finally, these substituents, because of their flexibility, allowed for control over surface pressure of the dyad Langmuir films, a key factor determining their spacing between the Zn(TPPE) moieties within the film.

Table 1. Values of Area Per Molecule Determined from the $\pi-A$ Compression Isotherms for Langmuir Films of Zn(TPPE), C_{60}im, and the Zn(TPPE)-C_{60}im (1:1, mole: mole) Dyad Spread on the Water Subphase

	parameters of the $\pi-A$ compression isotherms			
	determined			estimated
Langmuir film[a]	$A_{0,1}$; $A_{0,2}$ (nm^2)	κ_1; κ_2 ($\times 10^{-2}$ m mN^{-1})	$\mu_\perp$ (D)	$A_{0,1}$; $A_{0,2}$ (nm^2)
C_{60}im	0.99; 0.87	2.61; 2.83	0.50; 0.56	1.38; 1.17
Zn(TPPE)	2.84; 2.09	6.38; 3.82	6.86; 9.25	~8.53; 1.85
Zn(TPPE)-C_{60}im	2.03; –	2.59; –	4.26; –	~8.53; 1.85

[a]The films were prepared by dispensing 150 μL samples of 0.1 mM Zn(TPPE) or Zn(TPPE)-C_{60}im in $CHCl_3$ or a 350 μL sample of 0.1 mM C_{60}im in $CHCl_3$.

Formation of the Zn(TPPE)-C_{60}im complex in solution was examined by the UV−vis spectroscopy titration of Zn(TPPE) with C_{60}im and the complex stability constant was determined. The molecular structure of the dyad as well as its HOMO and LUMO location were deduced from the DFT/(B3LYP/3-21G*) calculations. Next, the Zn(TPPE)-C_{60}im (1:1, mole: mole) donor−acceptor dyad and, separately, its components, were dissolved in chloroform used as a volatile solvent for spreading the Langmuir films. These films were characterized by simultaneous recording of the compression $\pi-A$ and $V-A$ isotherms as well as by BAM imaging. Properties of the Langmuir films of the dyad and, separately, of its components were then systematically investigated. Subsequently, the films were transferred onto different solid substrates using the LB technique. They were then characterized (i) spectroscopically by UV−vis spectroscopy, PM-IRRAS and XPS, (ii) microscopically by AFM imaging, (iii) electrochemically by DPV, and (iv) by the femtosecond transient absorption spectral measurements to establish the occurrence of the photoinduced electron transfer followed by (v) photoelectrochemical studies to evaluate its ability to generate photocurrent under different experimental conditions. Details of these experiments are presented below.

Computational and Spectroscopic Studies of the Zn(TPPE)-C_{60}im Dyad and Its Components in Solution. To optimize structure and determine electronic properties of the dyad, first, structures of both Zn(TPPE) and C_{60}im in vacuum were optimized, separately, to a stationary point on the Born−Oppenheimer potential energy surface with the DFT method at the B3LYP/3-21G* level using the Gaussian 09 software. Subsequently, structure of the Zn(TPPE)-C_{60}im dyad was optimized under the same conditions. To this end, both components, i.e., Zn(TPPE) and C_{60}im, were allowed to interact to form a bond between the Zn atom of Zn(TPPE) and the nitrogen atom of the imidazole moiety of C_{60}im. The length of this bond was calculated to be 2.007 Å. Notably, the Zn atom is slightly pulled out of the macrocycle plane toward the C_{60}im ligand. These calculation results are in agreement with calculations and crystal structure determinations already reported by us for similar compounds.[44,45]

In agreement with our earlier reports,[44,45] the present calculations indicate that the highest occupied molecular orbital (HOMO) is delocalized over the Zn(TPPE) macrocycle with the electron density neither on the ether peripheral substituents nor on the fullerene cage. Similarly, the lowest unoccupied molecular orbital (LUMO) was localized on the fullerene cage of the C_{60}im moiety (see Scheme S1 in the Supporting Information). Thus, the electron donor features of Zn(TPPE) and the electron acceptor feature of C_{60}im of the Zn(TPPE)-C_{60}im dyad were established. Moreover, the calculations yielded values and orientation of dipole moments of the dyad component molecules alone as well as of the dyad molecule (Scheme S2 and Table S1 in the Supporting Information). Noticeably, the dipole moment of the Zn(TPPE) molecule is relatively small and located in the Zn(TPPE) macrocycle plane, as should be expected for the highly symmetrical molecule. The direction of the dipole moment for the C_{60}im molecule is almost perpendicular to the long axis of the benzene-imidazole moiety. Formation of the dyad leads to the 2-fold increase of the dipole moment value. Additionally, the dipole moment direction is then clearly perpendicular to the phthalocyanine macrocycle plane.

The Zn(TPPE) donor was titrated with the C_{60}im acceptor using UV−vis spectroscopy in order to determine the stability constant of the Zn(TPPE)-C_{60}im complex formed in solution and to confirm its 1:1 stoichiometry (see Figure S2a in the Supporting Information). The consecutive addition of 3 and 5 μL of 1,2-dichlorobenzene solution samples of the C_{60}im ligand to the Zn(TPPE) solution of 1,2-dichlorobenzene caused the increase of absorbance of the Soret band of Zn(TPPE) at λ = 685 nm. From the observed absorbance change vs concentration of C_{60}im, the Zn(TPPE)-to-C_{60}im mole ratio was determined as 1:1 (see Figure S2b in the Supporting Information). The stability constant of the Zn(TPPE)-C_{60}im (1:1, mole: mole) complex in solution was, $K_s^s = 1.05 \times 10^5$ M^{-1} whose magnitude was close to those earlier reported for the zinc phthalocyanine-C_{60}im dyads (Figure S2c in the Supporting Information).[46] An additional qualitative evidence of the dyad formation was provided by the XPS experiment (not shown). That is, the binding energy peak of the Zn $2p_{3/2}$ electron slightly shifted toward lower energies and the full-width at half measure of this peak increased upon formation of the dyad.

Characterization of Langmuir Films. The Langmuir technique with simultaneous measurement of surface pressure and surface potential vs area per molecule is a convenient tool for controlling and studying molecular organization of monolayers at the air−water interface. The $\pi-A$ compression isotherm provides information on the area per molecule at zero pressure, A_0, and dynamic compressibility, κ, of the film. Here, the A_0 values were determined from the intercept of the slope tangents of the isotherms with abscissa at zero pressure (Table 1). The dynamic compressibility was determined using eq 1.

$$\kappa = -\frac{1}{A_0}\left(\frac{\partial A}{\partial \pi}\right)_T \quad (1)$$

Here, A is the area per molecule at a given surface pressure whereas $(\partial A/\partial \pi)$ is the inverse of the slope of the compression isotherm for a given phase and T is temperature in kelvins. The

reciprocal of the κ value serves to identify the Langmuir film phase.[47]

Similarly to our former studies,[39] there were two inflections in the π–A isotherm for the C_{60}im Langmuir film (curve 2 in Figure 1a), i.e., one at $\pi \approx 10$ and the other at $\pi \approx 13.8$ mN

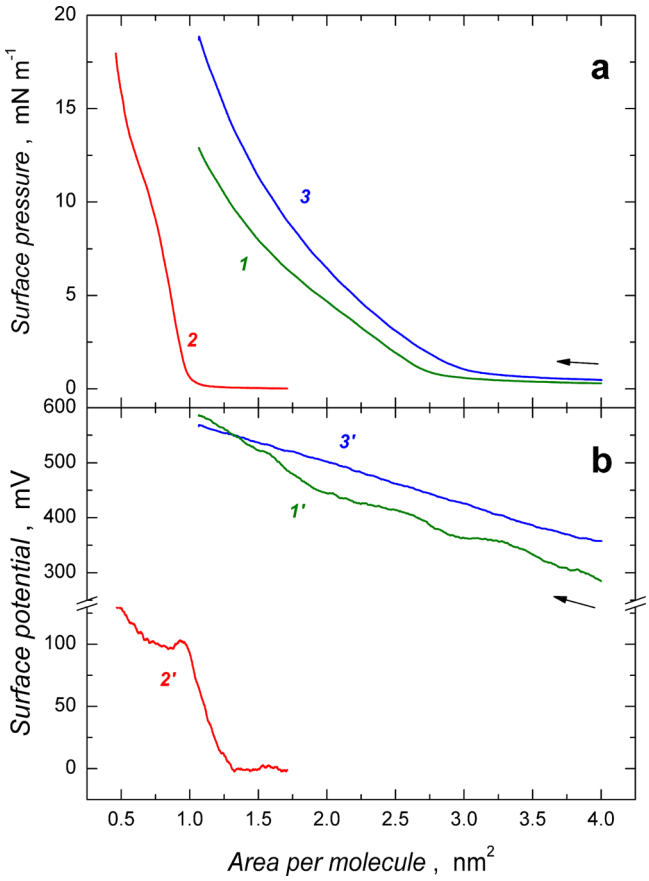

Figure 1. Compression isotherms of (a) surface pressure and (b) surface potential vs area per molecule for (1, 1′) 15 nanomoles of Zn(TPPE), (2, 2′), 35 nanomoles of C_{60}im, and (3, 3′) 15 nanomoles of the Zn(TPPE):C_{60}im (1:1, mole: mole) complex spread on the water subphase.

m^{-1}. These inflections resulted in two values of the area per molecule, i.e., $A_{0,1}$ and $A_{0,2}$, respectively (Table 1). They may be ascribed to two different orientations of C_{60}im molecules in the Langmuir film during its compression. Under the same conditions, inflections in the π–A isotherms for films of both the Zn(TPPE) and the Zn(TPPE)-C_{60}im dyad were ill-developed (curves 1 and 3 in Figure 1a) at $\pi \approx 8.5$ and $\pi \approx 10.6$ mN m^{-1}, respectively. These inflections are similar for both latter isotherms but they differ from that for the C_{60}im isotherm. Therefore, they presumably reflect orientation changes of the Zn(TPPE) rather than C_{60}im molecules in the dyad film. For Zn(TPPE), two values of area per molecule were determined. However, only one phase was well-developed for the Zn(TPPE)-C_{60}im dyad and the corresponding A_0 value was determined (curves 1 and 3 in Figure 1a, and Table 1).

The stability test of the Zn(TPPE)-C_{60}im Langmuir film (see Figure S3 in the Supporting Information) and dynamic compressibility provided information on the extent of aggregation of molecules in a monolayer phase. The C_{60}im Langmuir film revealed compressibility characteristic of the liquid expanded and liquid condensed phase for the $A_{0,1}$ and $A_{0,2}$ value, respectively (Table 1). The extent of aggregation of the Langmuir film of the Zn(TPPE) molecules in the liquid expanded phase suggests that the peripheral ether substituents were floating on the water surface rather than were immersed in it and that molecules mutually interacted during the compression. The Zn(TPPE)-C_{60}im dyad film demonstrated additive properties of the films of the Zn(TPPE) and C_{60}im components. However, rigidity of the dyad film was higher than that of the film of Zn(TPPE) and similar to that of the C_{60}im film.

The free energy gain due to dyad formation ($\Delta G_{\mathrm{dyad,film}}$) was calculated according to eq 2

$$\Delta G_{\mathrm{dyad,film}} = N_a\left(\int_0^{\pi_0} A_{\mathrm{dyad}}(\pi)d\pi - \int_0^{\pi_0} A_{\mathrm{Zn(TPPE)}}(\pi)d\pi - \int_0^{\pi_0} A_{\mathrm{C_{60}im}}(\pi)d\pi\right) \quad (2)$$

where N_a is the Avogadro constant, whereas A_{dyad}, $A_{\mathrm{Zn(TPPE)}}$, and $A_{\mathrm{C_{60}im}}$ are the area under the function $A(\pi)$ for the dyad, Zn(TPPE), and C_{60}im, respectively. The determined $\Delta G_{\mathrm{dyad,film}}$ value is -1.76 kJ mol^{-1}. Keeping in mind that $\Delta G = -RT \ln K_s^f$, we calculated the stability constant of the dyad in the Langmuir film, $K_s^f = 2.03$ M^{-1}. This value is much lower than that for the Zn(TPPE)-C_{60}im dyad in 1,2-dichlorobenzene. This discrepancy may be caused by solubility of neither the Zn(TPPE) nor C_{60}im in water on the one hand and by neglecting the mixing of the monolayer on the other.

The V–A isotherm, recorded simultaneously with the π–A isotherm, provides a deeper insight into orientation changes of molecules in a Langmuir film during its compression. The use of the Helmholtz relation, eq 3, allows for determination of the dipole moment component normal to the interphase plane, $\mu_\perp$

$$\mu_\perp = \varepsilon_0 \varepsilon A \Delta V \quad (3)$$

where ε_0 and ε are electric permittivity of free space and the film, respectively. An approximate value of electric permittivity for the Zn(TPPE) film, $\varepsilon_{\mathrm{Zn(TPPE)}} \cong 15$, was estimated as an average (1:4, mole:mole) of that for Zn phthalocyanine (ZnPc), $\varepsilon_{\mathrm{ZnPc}} = 8$,[48] and that for ethylene glycol monomethyl ether (EGME), $\varepsilon_{\mathrm{EGME}} = 16.9$.[49] The value of electric permittivity for the dyad, $\varepsilon_{\mathrm{Zn(TPPE)\text{-}C_{60}im}} \cong 10$, was estimated as an average of those for the Zn(TPPE) and C_{60} ($\varepsilon_{C_{60}} = 5$).[50]

Apparently, the measurement of surface potential as a function of area per molecule is more sensitive to the change of the molecule orientation than that of the surface pressure. That is, surface potential of the Langmuir film of C_{60}im in the V–A isotherm started to raise at a much higher A value than the surface pressure did in the corresponding π–A isotherm (curves 2 and 2′ in Figure 1a and 1b, respectively). This behavior indicates a phase transition in the C_{60}im film from the gaseous phase to the consecutively formed two liquid expanded phases of dynamic compressibility values of $\kappa_1 = 2.61 \times 10^{-2}$ and $\kappa_2 = 2.83 \times 10^{-2}$ m mN^{-1}. This transition is clearly illustrated by the surface potential change in the area per molecule range of $0.96 \leq A \leq 1.3$ nm^2, corresponding to the surface pressure range of $0.0 \leq \pi \leq 1.2$ mN m^{-1}, respectively. Simultaneously, the linear increase of surface pressure with the area per molecule decrease of the Langmuir film of C_{60}im above 10 mN m^{-1} was accompanied by a linear growth of the surface potential followed by development of a plateau. This growth may indicate formation of a bi- or multilayer C_{60}im film (presumably by pushing up the C_{60}im molecules out of the

dx.doi.org/10.1021/am501446g | ACS Appl. Mater. Interfaces 2014, 6, 8688–8701

monolayer plane) or the molecule orientation change. From the above measurements, the dipole moment component of the C_{60}im molecule perpendicular to the subphase surface is relatively low, being $\mu_{\perp} \leq 0.56$ D (Table 1). The total dipole moment of the C_{60}im molecule, calculated by the DFT method at the B3LYP/3-21G* level, is 4.46 D (see Table S1 in the Supporting Information) and its component parallel to the long axis of the benzene-imidazole moiety is 1.7 D. Taking results of these calculations into account, one can conclude that the C_{60}im molecule is either oriented on the subphase with the long axis of the benzene-imidazole moiety tilted at 40−50° with respect to normal to the subphase surface or is laying on its side.

Apparently, the π−A and V−A isotherms for Zn(TPPE) (curves 1 and 1′ in Figure 1a and 1b, respectively) are different than those for C_{60}im. That is, surface pressure started to grow at the beginning of compression in the Langmuir film of the former. At the surface pressure, $\pi \leq 5$ mN m^{-1}, i.e., when the first phase was formed with $A_{0,1} = 2.83$ nm^2, the Langmuir film of Zn(TPPE), with $\kappa_1 = 6.46 \times 10^{-2}$ m mN^{-1}, revealed protein-like behavior.[51] With the increase in surface pressure, the phase transition was ill defined. It resulted in formation of a liquid-expanded ($\kappa_2 = 3.91 \times 10^{-2}$ m mN^{-1}) Langmuir film with $A_{0,2} = 2.13$ nm^2. Presumably, mutual repulsion of peripheral ether substituents of the neighboring Zn(TPPE) macrocycles still predominated and compactness of the film substantially increased with the time of compression at constant surface pressure. An indirect proof of that may provide a continuous decrease of separation of the Langmuir trough barriers necessary for maintaining the selected surface pressure constant. The surface pressure vs time transient confirmed this inference (see Figure S3 in the Supporting Information). Surface potential of the Zn(TPPE) Langmuir film was growing linearly with the decrease of the area per molecule until $A \approx 1$ nm^2. Further increase of surface pressure resulted in collapse of the film and decrease of surface potential to its initial value (not shown).

The π−A and V−A isotherms for the film of the Zn(TPPE)-C_{60}im dyad (curves 3 and 3′ in Figure 1a and 1b, respectively) reflect interfacial behavior of Zn(TPPE). However, the first (protein-like) phase at low surface pressure was not formed. The liquid-expanded phase was formed at $\pi > 14$ mN m^{-1} with $A_{0,1} = 2.59$ nm^2. This phase corresponds to that of the Zn(TPPE) film formed under the same conditions. Interestingly, the value of $\mu_{\perp}$ estimated from the V−A isotherm is quite high (Table 1). However, the computed value of the total dipole moment of the Zn(TPPE) molecule is rather low (μ = 0.58 D) (see Table S1 in the Supporting Information) and positioned in plane of the macrocycle. However, this value was computed for the molecule with the ether peripheral chains completely spread in plane of the macrocycle. If these chains are tilted with respect to this plane, the dipole moment is higher and directed perpendicularly to this plane. Therefore, the determined value of $\mu_{\perp}$ supports the geometry of the Zn(TPPE) porphyrin molecule laying flat on the subphase surface with peripheral ether chains immersed in the water subphase, perpendicularly to this surface.

The shape of both the π−A and V−A isotherms for the Zn(TPPE)-C_{60}im film suggests mutual repulsion of peripheral ether substituents of the Zn(TPPE) macrocycles. At low surface pressure, the macrocycle planes of Zn(TPPE) are orientated rather in parallel with respect to the water−air interface plane. At this low surface pressure, the C_{60}im ligand points to air with its C_{60} cage because of hydrophobicity of this cage. Compression of the Langmuir film of the Zn(TPPE)-C_{60}im dyad results in, first, reorganization of the flexible peripheral ether substituents of the Zn(TPPE) moiety, and then reorientation of the dyad molecules with respect to the interface plane resulting in the formation of a J-type film structure. In this case, the $\mu_{\perp}$ value, estimated from the V−A isotherm, reached 4.26 D (Table 1). On the other hand, the computed value of the total dipole moment of the dyad is 8.69 D (Table S1 in the Supporting Information) and its component perpendicular to the macrocycle plane is 8.5 D, whereas the component located in the plane of the macrocycle is 1.8 D. Therefore, the total dipole moment is nearly perpendicular to the Zn(TPPE) macrocycle plane. However, the optimized Zn(TPPE) structure exhibited the ether chains laying in the macrocycle plane. This geometry may not necessarily be the case for the Langmuir film. This inference leads to the conclusion that, importantly, the peripheral ether chains of the Zn(TPPE) moiety in the dyad are either tilted against the subphase plane at ∼60° or they are immersed in the subphase in the opposite direction than that of the C_{60}im acceptor. Moreover, this orientation would manifest itself with a lower total value of the dipole moment. In view of the results of PM-IRRAS measurements (see below), the former possibility is excluded, and consecutively, the latter molecular arrangement is most probable.

The Zn(TPPE), C_{60}im, and Zn(TPPE)-C_{60}im Langmuir films were BAM imaged at surface pressure of 0, 1, and 10 mN m^{-1} (Figure 2). A foamy Zn(TPPE) film was formed even at π = 0 mN m^{-1} (Figure 2a). It was smoother and more compact the higher the surface pressure was. At π = 10 mN m^{-1} (Figure 2c), circular domains were formed and thickness of the film increased spatially. Bright spots indicated collapse points of the film (Figure 2c). At surface pressure of 0 and 1 mN m^{-1}, the film of C_{60}im was composed of aggregates and did not cover completely the surface of the subphase (Figure 2a′ and b′). This behavior is consistent with the determined A_0 values, which were lower than that estimated for the C_{60}im molecule (Table 1). However, a uniform film was formed at 10 mN m^{-1} (Figure 2c′). The Zn(TPPE)-C_{60}im film images were different from those of the pristine Zn(TPPE) and C_{60}im films. That is, circular domains were formed even at π = 0 (Figure 2a″). The distance between them decreased with the surface pressure increase (Figure 2b″). At π = 10 mN m^{-1}, islands with distinguishable areas of different thickness were formed (Figure 2c″). The BAM images for the dyad film at π = 0 and 1 mN m^{-1} were similar to that for the Zn(TPPE) film at π = 10 mN m^{-1}.

Characterization of the Langmuir−Blodgett Films. For the highest possible photoelectrochemical efficiency of the LB films of organic electron donor−acceptor dyads, conditions of the LB transfer of Langmuir films of the dyad onto transparent electrodes should be optimized. Two important factors governing photoelectrochemical efficiency of the LB films of the Zn(TPPE)-C_{60}im dyad include proper organization of the dyad molecules in the film and sufficiently high light absorbance. On the one hand, the higher surface pressure of transfer of the Langmuir film the denser is the packing of the dyad molecules in the resulting LB film and higher is its light absorbance. This is because then the film contains more of the photoactive molecular centers. On the other, however, high surface pressure results in unfavorable changes in the Zn(TPPE)-C_{60}im dyad orientation with respect to the substrate

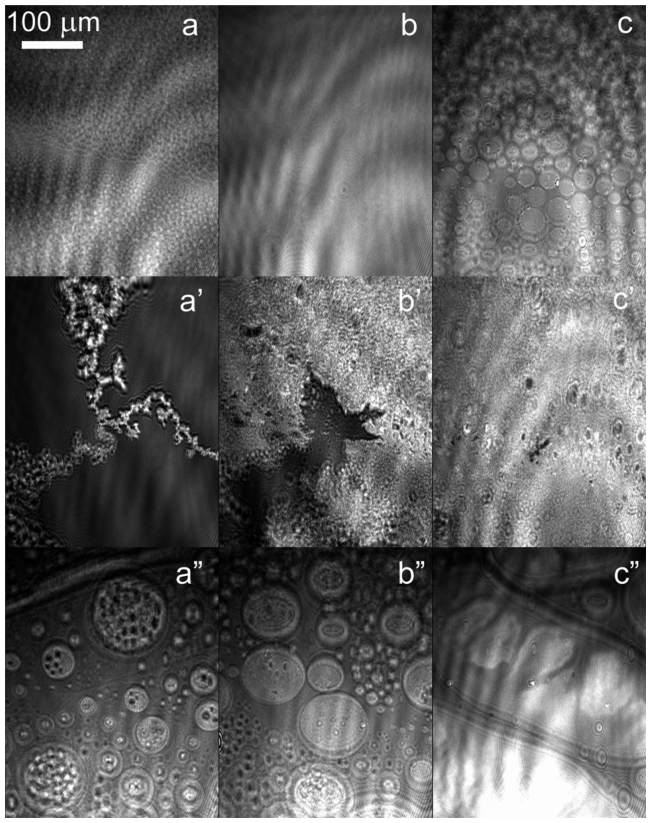

Figure 2. Brewster angle microscopy images of the Langmuir films of (a, b, c) Zn(TPPE), (a′, b′, c′) C_{60}im, and (a″, b″, c″) the Zn(TPPE)-C_{60}im (1:1, mole: mole) dyad spread on the water subphase. The films were imaged at surface pressure of (a, a′, a″) 0, (b, b′, b″) 1, and (c, c′, c″) 10 mN m^{-1}.

surface to result in random orientation and in shrinking the distance between the neighboring bulky Zn(TPPE) electron-donor moieties in the transferred film (see Scheme S3 in the Supporting Information). Although, advantageously, light absorption of highly compressed film is higher, the unfavorable random orientation of the dyad molecules in it may result in an inefficient charge transfer within the film.

The Langmuir films of the dyad were LB transferred onto the FTO substrate by vertical immersion, and then withdrawal of the substrate. For that, the films were transferred at different values of surface pressure, transfer rate, and number of transfers, onto hydrophobic or hydrophilic substrate, upon its immersion or withdrawal for the transfer of the first layer. The FTO-coated glass slides were hydrophobized by chemical modification with trimethoxyphenylsilane. The highly hydrophilic FTO slides were prepared by oxygen plasma treatment, whereas the FTO slides with controlled hydrophilicity were prepared by mixed argon-oxygen plasma treatment at different values of plasma power and exposition time.

The dyad Langmuir film was successfully transferred, using the LB technique, onto the hydrophobic FTO glass slide by consecutive immersion and withdrawal of this slide substrate. The transfer resulted in the Y-type organized LB film on the hydrophobic substrate (see Scheme S4a in the Supporting Information). Interestingly, the transfer ratio for the dyad Langmuir film transferred onto a hydrophilic FTO surface resulted in the Y-type LB film on the hydrophilic substrate (see Scheme S4b in the Supporting Information) was close to null. In the latter experiment, the first layer of the LB film was deposited by withdrawal of an initially immersed hydrophilic FTO slide. Surprisingly, it was possible to transfer the Zn(TPPE) Langmuir film onto both hydrophilic and hydrophobic solid substrates only in the presence of the C_{60}im acceptor in the Langmuir film, i.e., if the donor−acceptor dyad was initially formed in the air−water interface. This result signifies that the hydrophobic C_{60}im acceptor moiety of the dyad was facing the substrate. An attempt to transfer the X-type organized Zn(TPPE)-C_{60}im dyad Langmuir film (see Scheme S4c in the Supporting Information) onto the hydrophobic FTO substrate, mounted in parallel to the Langmuir film plane using the Langmuir-Schaeffer technique, appeared inefficient. Therefore, further transfer optimization was focused on the (i) transfer rate, (ii) transfer pressure, and (iii) number of transfers of the dyad LB film depicted in Scheme S4a in the Supporting Information. All these transfer parameters were explored in order to find optimum transfer conditions.

The lower limit of the transfer rate was governed by stability of the Langmuir film (see Figure S3 in the Supporting Information) and the evaporation rate of the water subphase. For preserving film uniformity, the transfer rate should be relatively high. The 5 mm min^{-1} transfer rate was selected to compromise between the values sufficiently low to keep dyads in the LB film uniform on the one hand and sufficiently high to maintain surface pressure constant on the other. The film transfer at 15 mm min^{-1} was substantially less efficient, whereas films transferred at too high transfer rate of 30 mm min^{-1} revealed nearly no photocurrent at all (not shown). Apparently, the molecular order of the LB films transferred at such a high rate was not favorable for efficient photovoltaics.

The surface pressure applied for transfer of the Langmuir film of the Zn(TPPE)-C_{60}im dyad should compromise between that enabling high absorption of light and that of most favorable organization of the dyad molecules in the resulting LB film. Herein, this compromised surface pressure range was relatively narrow. That is, the dyad film transferred at 8 mN m^{-1} resulted in unfavorably low light absorbing LB films on the one hand and the transfer at high surface pressure of 24 mN m^{-1} resulted in no photocurrent. Apparently, the LB films transferred at 10 mN m^{-1} best performed in photoelectrochemical experiments. Although the films transferred at higher surface pressure, e.g., 15 mN m^{-1}, absorbed more light, they generated lower photocurrents.

Finally, the influence of the number of transfers of the Langmuir films on the photoelectrochemical performance of the resulting LB films was examined. Here, the limiting factor was the decrease of both the transfer ratio and the organization of the dyad molecules in the LB film with the number of transfers. For the trimethoxyphenylsilane hydrophobized FTO slide, the average transfer ratio exceeded 100% for the first 60 transfer cycles (see Figure S4 in the Supporting Information). This effect might be caused by rearranging peripheral ether substituents of the Zn(TPPE) molecules with time. That is, the film might become more compact and the distance between the trough barriers decreased (see Figure S3 in the Supporting Information). This behavior resulted in the decrease of area of the Langmuir film, additional to that characteristic of the LB transfer, thus artificially inflating the transfer ratio. Generally, the higher number of transfers the higher was the light absorption of the LB films and higher the photoelectrochemical performance. Saturation of these parameters was not reached even after 250 transfers.

The LB transfer of the Zn(TPPE) Langmuir film was successful only in the presence of the C_{60}im ligand (curve 3″ in Figure 3c). The LB transfer of the pristine Zn(TPPE) was

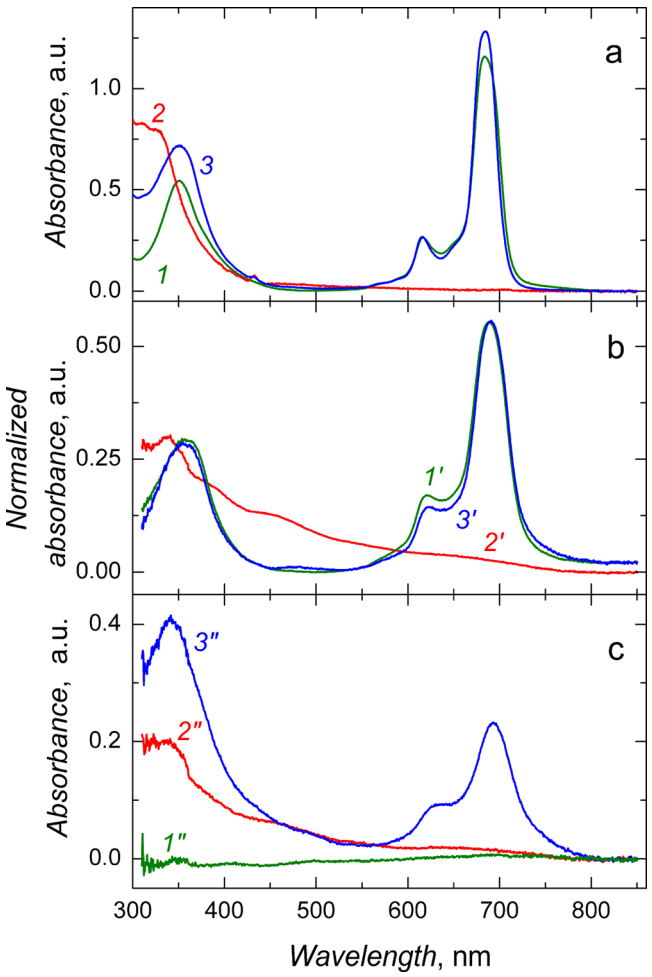

Figure 3. UV−vis absorbance spectra for (1, 1′, 1″) Zn(TPPE), (2, 2′, 2″) C_{60}im, and (3, 3′, 3″) the Zn(TPPE)-C_{60}im, (1:1, mole: mole) dyad in (a) 1,2-dichlorobenzene, (b) the films drop coated onto the FTO glass slides, and (c) the LB films transferred onto the FTO glass slides.

successful onto neither the hydrophilic nor hydrophobic substrate (curve 1″ in Figure 3c). The ratio of absorbance of the peak at ∼685 nm to that at ∼350 nm for the dyad in solution or in the film drop cast onto an FTO slide (curves 3 and 3′ in a and b in Figure 3, respectively) to that for the LB transferred film (curve 3″ in Figure 3c), is reversed. This reversed ratio suggests a different relative ratio of the two moieties of the dyad in solution and in a multilayer LB film. Higher absorbance at ∼330 nm indicates the excess of the C_{60}im moiety in the LB transferred dyad film. The reason for this excess may be partial dissociation of the dyad during the transfer.

To confirm the dyad orientation and to evaluate the molecular order in the LB films transferred onto the FTO substrate at different surface pressures, we recorded the ATR-FTIR and PM-IRRAS spectra of the dyad multilayer LB films (Figure 4a). For that, the dyad films were transferred onto the (Au-over-Ti)-coated glass slides to be suitable for the PM-IRRAS measurements. The LB dyad films were prepared in the course of 100 transfers at the 10 mN m^{-1} surface pressure and the 5 mm min^{-1} transfer rate. For comparison, the PM-IRRAS and ATR-FTIR spectra of both the C_{60}im (curve 1 in Figure 4b) and Zn(TPPE) (curve 2 in Figure 4b) powders were also recorded. The PM-IRAS spectrum is dominated by the Zn(TTPE) bands which, also in the powder ATR-FTIR spectrum, are stronger than those in the spectrum of C_{60}im. Nevertheless, two bands characteristic of C_{60}im at 1526 and 1180 cm^{-1} are clearly seen in the spectrum of the LB film of the dyad, thus confirming its presence in the film. The band at 1526 cm^{-1} corresponds to the imidazole ring antisymmetric vibration[39] while that at 1180 cm^{-1} can be assigned to the ω_3 (F_{1u}) C_{60} cage vibration.[39] Interestingly, the former band is stronger than the latter. Their transition dipole moments are perpendicular to each other with the imidazole vibration dipole moment aligned with the long axis of the benzene-imidazole moiety of the C_{60}im. Apparently, the C_{60}im molecule is oriented with the long axis of its benzene-imidazole moiety almost perpendicular to the substrate surface and only slightly tilted against the normal to the substrate surface, as indicated in Scheme S1b and Scheme S3a in the Supporting Informaiton.

To gain a deeper insight into the Zn(TPPE) macrocycle orientation in the film, we analyzed two groups of bands. One of them contains vibrations at 2963, 2924, 2852, and 1092 cm^{-1}. Those bands can be assigned to the vibrations of asymmetric $-CH_2-$ and $-CH_3$ stretching, symmetric $-CH_2$ stretching, and C−O−C stretching, respectively.[52,53] The analysis of these bands reveals orientation of the peripheral ether substituents of the Zn(TPPE) molecule. The second group involves bands at 1607, 1486, 1465, 1241, and 1122 cm^{-1} corresponding to the aromatic C═C stretching vibration, two asymmetric benzene ring stretching vibrations, and phthalocyanine macrocycle vibrations, macrocycle "breathing", as well as the C−H benzene moiety in-plane "wagging" vibrations, respectively.[54] This group of bands allows to discern orientation of the Zn(TPPE) macrocycle in the film. For the first group of vibrations, the transition dipole moments for the 2963 and 1092 cm^{-1} vibrations are aligned with the long axis of the peripheral ether chains.[55] However, transition dipole moments of the vibrations at 2924 and 2852 cm^{-1} are perpendicular to the long axis of the ether chains.[55] In the recorded PM-IRRAS spectrum for the dyad LB film (Figure 4a), one can clearly see that the peak at 2924 cm^{-1} dominates this region of the spectrum, and in fact the whole spectrum. This domination is in contrast to that observed in the ATR-FTIR spectrum of randomly oriented Zn(TPPE) molecules (curve 2 in Figure 4b). However, peaks at 2852 and 2963 cm^{-1} are also well developed. This behavior clearly indicates that, importantly, the ether chains are tilted against the normal to the Au-over-Ti substrate surface. The same conclusion could be drawn from the variations in intensity of the peak at 1092 cm^{-1} corresponding to the C−O−C stretching. This band is the strongest in the ATR-FTIR spectrum of the randomly oriented Zn(TPPE) molecules (curve 2 in Figure 4b) while its relative intensity with respect to other bands in the PM-IRRAS spectrum of the dyad LB film (Figure 4a) is largely decreased. All these inferences allow concluding that the peripheral ether chains are not parallel to the substrate surface although they are markedly tilted against normal to this surface.

Similar spectral analysis was performed for the second group of the bands corresponding to vibrations of the Zn(TPPE) macrocycle. Transition dipole moments of all studied bands of this group are in-plane of the macrocycle. If the macrocycle

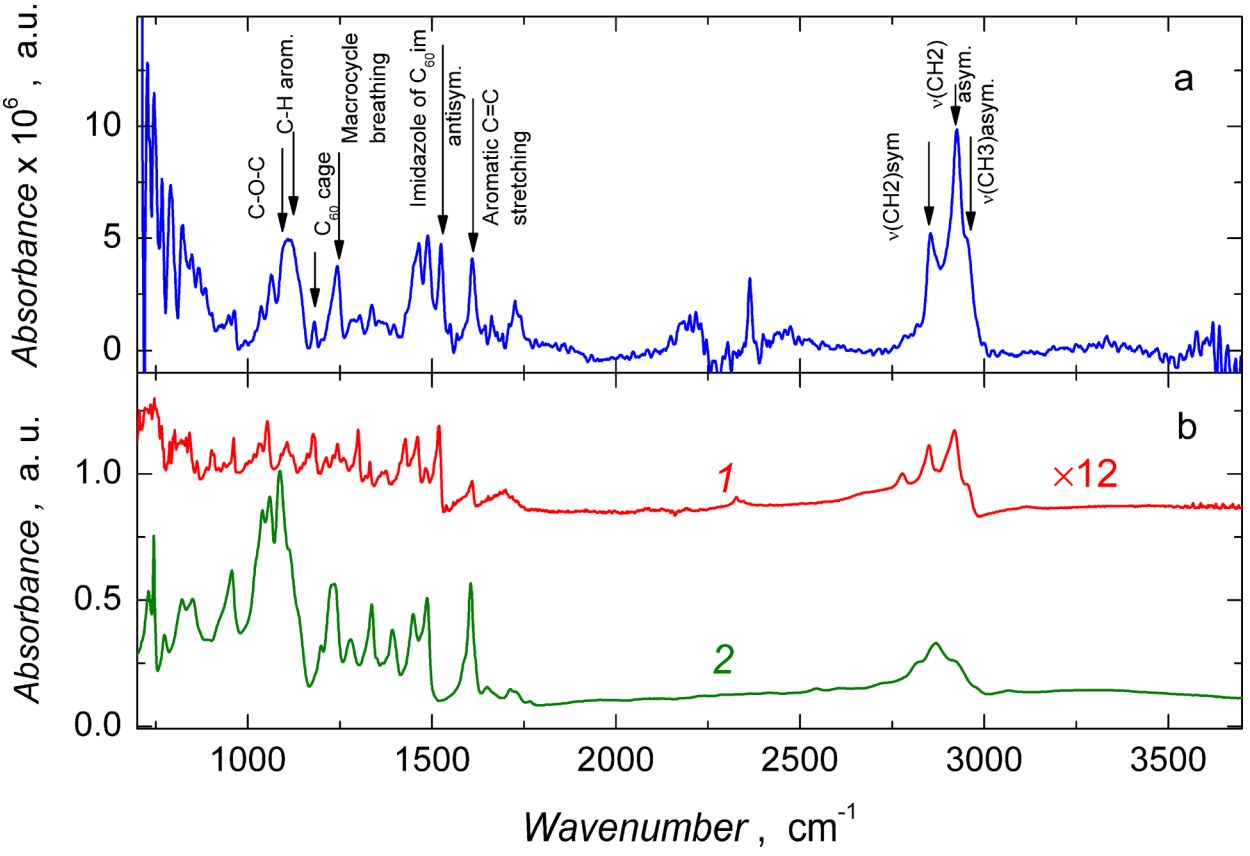

Figure 4. The (a) PM-IRRAS spectrum for the LB film of the Zn(TPPE)-C_{60}im dyad transferred by 100 immersions at 10 mN m^{-1} onto Au-over-Ti coated glass slide with the transfer rate of 5 mm min^{-1}, recorded at incidence angle of 83°. The (b) ATR IR spectra for powders of (1) C_{60}im and (2) Zn(TPPE).

plane of the Zn(TPPE) molecule was parallel to the surface of the substrate, intensities of the bands in the spectrum of the dyad LB film (curve in Figure 4a) would be much lower compared to those in the ATR-FTIR spectrum of randomly oriented Zn(TPPE) molecules (curve 2 in Figure 4b). This is the case, indeed, as can be seen in panels a and b in Figure 4. However, the discussed phthalocyanine bands are still visible in the spectrum. This behavior permits concluding that the phthalocyanine macrocycles in the LB film are strongly tilted against the normal to the substrate surface laying almost, but not perfectly, flat on this surface.

The PM-IRRAS spectrum of the LB film of the dyad transferred at 24 mN m^{-1} (not shown) is not much different from that for the film transferred at 10 mN m^{-1} indicating that the molecules in the film do not undergo dramatic rearrangements. However, the films transferred at 24 mN m^{-1} do not produce photocurrent upon light irradiation. Accordingly, thorough comparison of ratios of intensities of different vibrations shows subtle changes in orientation of the molecules. A lower intensity ratio of the bands at 1526 and 1180 cm^{-1} indicates that the tilt of the long axis of the benzene-imidazole moiety of C_{60}im is higher the higher is the transfer pressure. On the other hand, the peripheral ether chains of the Zn(TPPE) molecule are more perpendicular to the surface, as evidenced by the lower ratio of intensities of peaks at 2924 and 1092 cm^{-1}. Finally, the increase of intensity of the peak at 1123 cm^{-1} with the pressure increase compared to the peak at 1092 cm^{-1}, corresponding to the C−O−C stretching, indicates that the macrocycle becomes less tilted against the normal to the surface if the film is transferred at higher surface pressure. All the above considerations indicate that the dyads in the film transferred at 24 mN m^{-1} are more strongly tilted against the normal to the substrate surface compared to that in the film transferred at 10 mN m^{-1} adopting conformation depicted in Figure S4c in the Supporting Information. Moreover, the peripheral ether chains of the Zn(TPPE) molecule are then more perpendicular to the Au-over-Ti substrate surface.

AFM Imaging of the Dyad LB Film. The AFM imaged topography of the dyad LB film indicates that the film surface is not fully homogeneous (see Figure S5 in the Supporting Information). It exhibits some holes. However, the determined relative surface area (R_{sa}) for the bare Au-over-Ti coated glass slide (see Figure S5a in the Supporting Information) is higher than that for the coated with the dyad film, transferred by 50 immersions (see Figure S5b in the Supporting Information), being 1.027 and 1.009, respectively. Apparently, roughness of the multilayer LB film of the dyad is lower. Moreover, the true value of the film roughness might be even lower. The one determined is affected by roughness of the substrate of the LB film.

Electrochemical Characterization of Zn(TPPE), C_{60}im, and the Zn(TPPE)-C_{60}im Dyad. The DPV curves for the dyad and, separately, for its components in solution were recorded in order to determine precisely the formal redox potentials (see Figure S6 in the Supporting Information). The Zn(TPPE)-C_{60}im dyad shows reversible peaks 1′ through 5′ (curve c in Figure S6 in the Supporting Information) corresponding to those recorded both for the Zn(TPPE)

(peaks 1 and 2 in curve a, in Figure S6 in the Supporting Information) at the formal potential of $E^{0\prime}$ = +0.33 and −1.29 V, respectively. Moreover, there are peaks 3, 4, and 5 (curve b, in Figure S6 in the Supporting Information) at $E^{0\prime}$ = −0.77, −1.15, and −1.68 V, respectively, corresponding to the C_{60}im moiety. The Zn(TPPE) donor shows one irreversible broad peak at −1.09 V (curve a in Figure S6 in the Supporting Information). Formal potentials of the C_{60}im redox processes were not shifted after formation of the dyad (cf. peaks 3, 4, 5 and 3′, 4′, 5′ in curves b and c, in Figure S6 in the Supporting Information, respectively). However, the formal potential of the Zn(TPPE) redox process was then shifted by ∼10 mV (peaks 1 and 1′ in curves a and c, in Figure S6 in the Supporting Information, respectively). Peaks at −1.09 and −1.29 V for the Zn(TPPE) overlap the second reduction peak of C_{60}im (peaks 2′ and 4′ in Figure S6c in the Supporting Information).

Photoinduced Electron Transfer in the Zn(TPPE)-C_{60}im LB Film. To secure evidence for the formation of charge separated species upon photoexcitation of the Zn(TPPE)-C_{60}im LB film and to evaluate kinetics of charge separation and recombination, the femtosecond transient absorption spectroscopic measurements were performed. For this, a 400 nm laser light, with a 100 fs pulse width used as the excitation source, on the dyad LB films, transferred onto the trimethoxyphenylsilane hydrophobized FTO electrode, was used. Figure 5a shows transient spectra recorded at different delay times. Immediately after excitation, a positive peak at 525 nm characteristic of the S_0 to S_1 transition and a negative peak at 694 nm corresponding to the fluorescence emission of zinc phthalocyanine were observed. These peaks were accompanied by two peaks at 856 and 1020 nm corresponding, respectively, to the formation of the Zn(TPPE)$^{\cdot+}$ and C_{60}im$^{\cdot-}$ species, thus confirming the formation of an ion-pair radical within the Zn(TPPE)-C_{60}im LB film.[56,57] The time profile of the 856 nm band was analyzed to evaluate the kinetics of charge separation and recombination (Figure 5b). The determined rate constants of charge separation, k_{cs}, and charge recombination, k_{cr}, were 2.6×10^{11} s^{-1} and 9.7×10^{9} s^{-1}, respectively. The magnitude of k_{cs} indicates occurrence of efficient vectorial electron transfer whose time constant is close to that of the laser pulse. The magnitude of k_{cr} was by an order magnitude smaller, a general trend expected for tetrapyrrole-fullerene type dyads.[58]

Photoelectrochemical Properties of the Multilayer LB Film of the Zn(TPPE)-C_{60}im Dyad. The photoelectrochemical cell was assembled with the dyad LB film electrode illuminated from the solution side (see Scheme S5 in the Supporting Information). The effect of the parameters of the LB transfer, like hydrophobicity of the FTO substrate, the transfer rate and surface pressure as well as the number of transfers, on the photoelectrochemical performance of this electrode was investigated thoroughly. First, the current−potential (I−E) curves for the LB films of the dyad transferred at different values of surface pressure and transfer rate as well as for different supporting electrolyte and electron mediator solutions were recorded in the dark and under the AM1.5 light illumination. Positively or negatively charged electron mediators are preferred for the photoelectrode to work as the photocathode or photoanode, respectively. Therefore, methylviologen (MV^{2+})[59] and monoascorbate ($AscH^{-}$)[60] were selected for the photoelectrode to operate as the photocathode and photoanode, respectively (Scheme S5b and S5a in the Supporting Information, respectively). Remarkably, the photoanodic current was over an order of magnitude higher than the

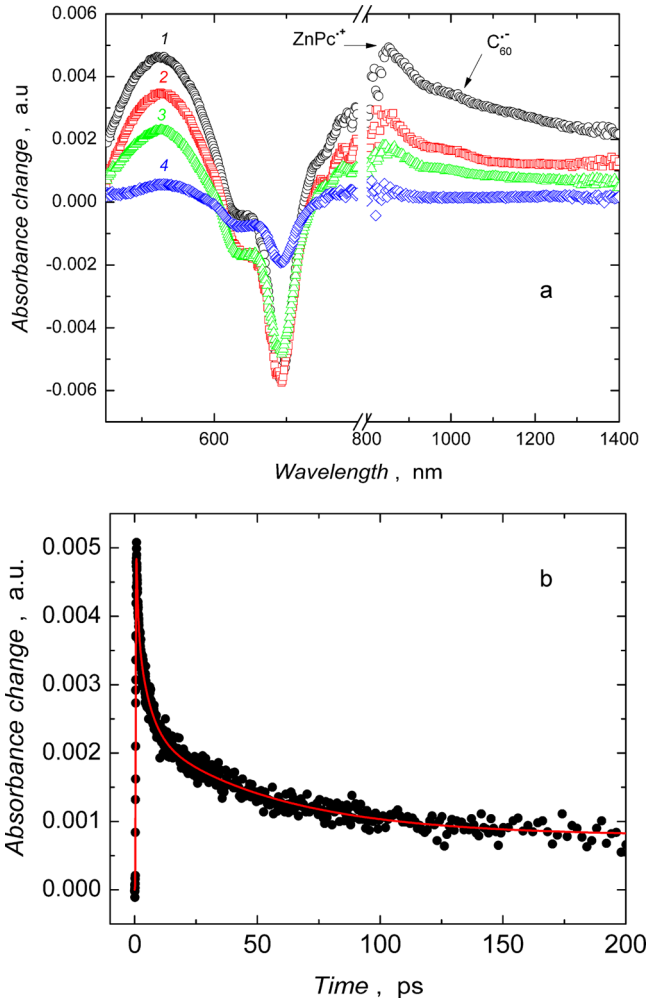

Figure 5. (a) Transient absorbance spectra of the Zn(TPPE)-C_{60}im LB film, transferred onto the trimethoxyphenylsilane hydrophobized FTO electrode by 100 immersions at 5 mm min^{-1}, after excitation at 400 nm with 100 fs pulses, recorded for (1) 0.830, (2) 7.66, (3) 33.8, and (4) 2298 ps. (b) Time profile of the transient absorbance band at 856 nm.

photocathodic current (curves 1 and 2 in Figure 6, respectively). The photoanodic and photocathodic current density was dependent on the potential applied and it was 61.6 μA cm^{-2} at +0.3 V in the solution of ascorbic acid and 5.7 μA cm^{-2} at −0.2 V in the solution of methylviologen. At pH ≈ 4.1, i.e., that equal to pK_{a1} of $AscH_2$, half of the acid molecules are dissociated forming a monoanionic mediator, $AscH^{-}$ (eq 4)

$$AscH_2 \underset{+H^+}{\overset{-H^+}{\rightleftharpoons}} AscH^- \underset{+H^+}{\overset{-H^+}{\rightleftharpoons}} Asc^{2-} \quad (p\mathit{K}_{a1}=4.1,\ p\mathit{K}_{a2}=11.8) \tag{4}$$

In the presence of the $AscH^{-}$ mediator, the proposed mechanism (see Scheme S5a in the Supporting Information) of the photoanodic activity of the FTO/[C_{60}im-Zn(TPPE) LB multilayer film] working electrode is, as follows. The first step of this mechanism involves the photoassisted intramolecular charge transfer within the dyad from the photoexcited Zn(TPPE) donor moiety to the C_{60}im acceptor moiety resulting in formation of the Zn(TPPE) cation radical and the C_{60}im anion radical, respectively (eq 5).

dx.doi.org/10.1021/am501446g | ACS Appl. Mater. Interfaces 2014, 6, 8688−8701

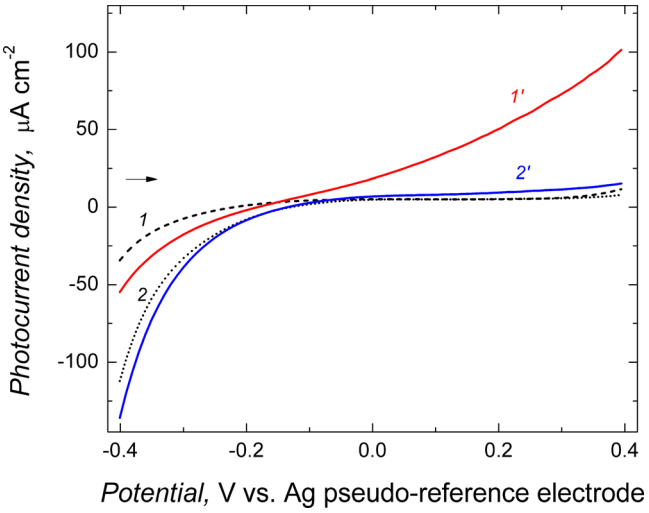

Figure 6. Photocurrent–potential characteristics of the trimethoxyphenylsilane hydrophobized FTO electrode, operating as the (1, 1′) photoanode and (2, 2′) photocathode, coated with the Zn(TPPE)-C_{60}im dyad LB film, transferred by 200 LB immersions, at the 5 mm min^{-1} transfer rate (1 and 2) in the dark and (1′ and 2′) under the AM1.5 light irradiation conditions in (1 and 1′) 1 mM ascorbic acid, in 0.1 M NaH_2PO_4 (pH ≈ 4.1) and in (2 and 2′) 5 mM methylviologen, in 0.1 M Na_2SO_4 (pH ≈ 5.8), respectively.

$$\text{Zn(TPPE)-C}_{60}\text{im} \overset{h\nu}{\rightleftarrows} \text{Zn(TPPE)}^{\cdot+}\text{-C}_{60}^{\cdot-}\text{im} \quad (5)$$

Then, the extra electron on C_{60}im anion radical facing the hydrophobized surface travels through the FTO anode to the Pt cathode (eq 6).

$$\text{photoanode, FTO(-): Zn(TPPE)}^{\cdot+}\text{- C}_{60}^{\cdot-}\text{im} \overset{-e^-}{\underset{+e^-}{\rightleftarrows}} \text{[Zn(TPPE)}^{+}\text{- C}_{60}^{\cdot-}\text{im]}^{+} \quad (6)$$

Simultaneously, the ascorbate monoanion donates the electron to the Zn(TPPE)$^{\cdot}$ moiety of the dyad and it is oxidized that way to the AscH$^{\cdot}$ neutral radical (eq 7).[60]

$$\text{[Zn(TPPE)}^{\cdot+}\text{- C}_{60}^{\cdot-}\text{im]}^{+} + \text{AscH}^{-} \rightleftarrows \text{Zn(TPPE)- C}_{60}\text{im} + \text{AscH}^{\cdot} \quad (7)$$

The resulting radical, AscH$^{\cdot}$, is then electroreduced to AscH^{-} on the Pt cathode according to eq 8.

$$\text{cathode, Pt(+): AscH}^{\cdot} \overset{+e^-}{\underset{-e^-}{\rightleftarrows}} \text{AscH}^{-} \quad (8)$$

In consecutive I–E curves for the LB film of the dyad in the ascorbic acid solution, the photocurrent density increased (curves 2 through 6 in Figure S7 in the Supporting Information). Most likely, this increase was due to reorganization and restructuring of the film.

The proposed mechanism of the photocathodic performance of the photoelectrode requires the MV^{2+} presence and an opposite electron transfer through the cell. The first step, which is the intramolecular charge transfer within the dyad upon illuminations, is the same as that above (eq 5). However, next, the electron is donated by the $C_{60}^{\cdot-}$ moiety of the dyad to the cation, MV^{2+} (eq 9).

$$\text{Zn(TPPE)- C}_{60}^{\cdot-}\text{im} + \text{MV}^{2+} \rightleftarrows \text{[Zn(TPPE)}^{+}\text{- C}_{60}\text{im]}^{+} + \text{MV}^{\cdot+} \quad (9)$$

Then, the electron from the resulting cation radical, $MV^{\cdot+}$, is delivered to the Pt electrode, serving now as the anode, and $MV^{\cdot+}$ is electrooxidized to MV^{2+} (eq 10).

$$\text{anode, Pt(−): MV}^{\cdot+} \overset{-e^-}{\underset{+e^-}{\rightleftarrows}} \text{MV}^{2+} \quad (10)$$

Simultaneously, the [Zn(TPPE)-C_{60}im]$^+$ cation is electroreduced at the FTO photocathode (eq 11).

$$\text{photocathode, FTO(+): [Zn(TPPE)- C}_{60}\text{im]}^{+} \overset{+e^-}{\underset{-e^-}{\rightleftarrows}} \text{Zn(TPPE)- C}_{60}\text{im} \quad (11)$$

Photocurrent generation in the solution of AscH$^-$ or MV^{2+} was evaluated in the light switching on and off experiment. For the same film, the absolute value of photocurrent for the AscH$^-$ solution was over an order of magnitude higher than that for the MV^{2+} solution (curves 1 and 2 in Figure 7). The open

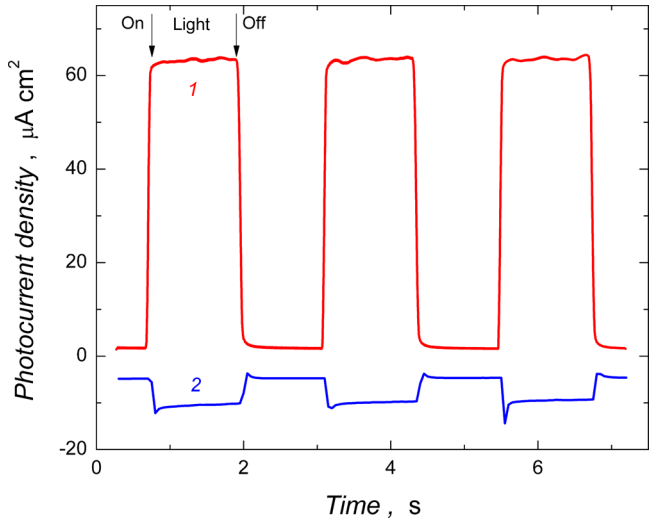

Figure 7. (1) Photoanodic and (2) phocathodic current density changes with time due to alternate light switching "on" and "off" for the Zn(TPPE)-C_{60}im LB film transferred by 200 immersions onto the trimethoxyphenylsilane hydrophobized FTO electrode at the 5 mm min^{-1} transfer rate for (1) 1 mM ascorbic acid, in 0.1 M NaH_2PO_4 (pH ≈ 4.1), and (2) 5 mM methylviologen in 0.1 M Na_2SO_4 (pH ≈ 5.8), recorded at +0.3 and −0.2 V vs the Ag pseudoreference electrode, respectively.

circuit potential, V_{oc}, for the light-irradiated cell was −0.207 V vs V_{oc} of the same cell in the dark for the LB film transferred by 200 immersions, at the 10 mN m^{-1} surface pressure and the 5 mm min^{-1} transfer rate, in the AscH$^-$ solution. The photocurrent density was higher the higher was the number of the LB transfers (not shown).

The incident photon-to-current conversion efficiency (IPCE) of the multilayer LB film of the Zn(TPPE)-C_{60}im dyad, transferred by 100 immersions at the applied potential of 0.0 V vs Ag pseudo-reference electrode, revealed maximum of nearly 0.3% at ∼400 nm (Figure 8). An elevated IPCE was observed at ∼690 nm corresponding to the visible band wavelength for the Zn(TPPE) moiety. However, the photovoltaic performance of this system was dependent on the film thickness and the

dx.doi.org/10.1021/am501446g | ACS Appl. Mater. Interfaces 2014, 6, 8688–8701

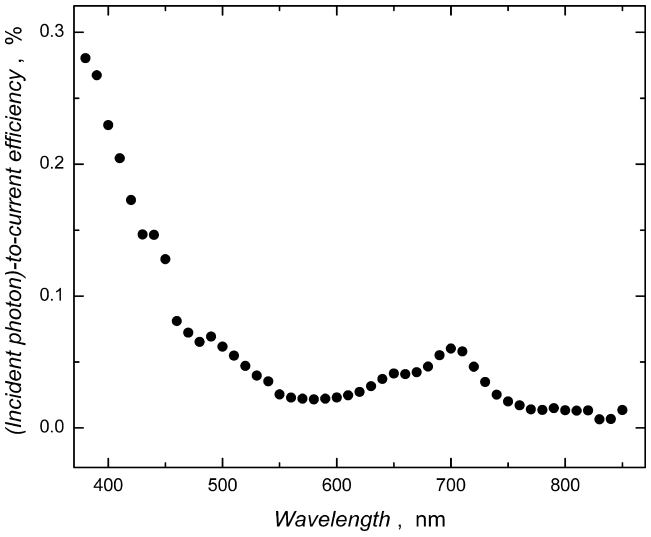

Figure 8. Incident photon-to-current conversion efficiency (IPCE) as a function of wavelength of incident light for the Zn(TPPE)-C_{60}im dyad multilayer LB film transferred onto the FTO optically transparent electrode, which was hydrophobized with trimethoxyphenylsilane, by 100 immersions in 1 mM ascorbic acid, in 0.1 M NaH_2PO_4 (pH ≈ 4.1).

saturation was not reached. That was because the photocurrent density was proportional to the number of LB transfers.

SUMMARY AND CONCLUSIONS

The Zn(TPPE)-C_{60}im (1:1, mole:mole) electron donor–acceptor dyad was supramolecularly self-assembled in a chloroform solution. The stability constant of the complex was determined by the UV–vis spectroscopy titration to be as high as $K_s^s = 1.05 \times 10^5$ M^{-1}. The Langmuir films of the dyad as well as those of its components were spread on the water subphase and the area per molecule was determined for the film of Zn(TPPE), C_{60}im, and the Zn(TPPE)-C_{60}im dyad. These values were lower than those estimated were. For the C_{60}im film, this effect was due to aggregation of molecules, whereas for the Zn(TPPE) film and the Zn(TPPE)-C_{60}im dyad film, it was due to high flexibility of peripheral alkyl ether substituents of the Zn(TPPE) molecules, resulting in low stability of the corresponding Langmuir films. The Langmuir films of the dyad were transferred onto solid substrates of different wettability to form multilayer LB films. The best performing in photoelectrochemical experiments LB films of the dyad were obtained by transferring them at the 5 mm min^{-1} transfer rate and the 10 mN m^{-1} surface pressure, onto the trimethoxyphenylsilane hydrophobized FTO substrates. The apparent transfer ratio exceeded 100% for both immersion and withdrawal for initial 60 LB transfers. Neither the LB transfer of the pristine Zn(TPPE) onto the hydrophobic or hydrophilic substrate nor that of the dyad onto the hydrophilic FTO substrate was successful. The resulting FTO electrode, coated with the dyad LB film, operated as either the photoanode or photocathode depending on the mediator used and on the potential applied; the photoanodic performance being higher. The photoanodic current density was ∼62 μA cm^{-2} at +0.3 V while the current density reached merely ∼6 μA cm^{-2} at −0.2 V of the applied bias potential when the working electrode operated as the photocathode. The PM-IRRAS measurements revealed that the phthalocyanine macrocycle plane of the dyad was slightly tilted with respect to the FTO surface plane whereas the peripheral ether substituents were highly tilted. The photocurrent density was proportional to the number of LB transfers but saturation with respect to the number of the transfers was not reached. The determined rate constants of the photoassisted charge separation, $k_{cs} = 2.6 \times 10^{11}$ s^{-1}, and charge recombination, $k_{cr} = 9.7 \times 10^9$ s^{-1}, indicated applicability of the dyad films in building photovoltaic devises. The IPCE value, determined for the film transferred by 100 immersions, was 0.3% at 0.0 V of the applied bias potential.

The present and our previous results of the research on similar photoelectrochemical systems[39−41] helped us to understand how the performance of these systems could be improved. The relevant recommendations include the following issues. (i) The extent of organization of the dyad molecules in the LB film should be as high as possible. (ii) The more hydrophobic the dyad the higher the quality of the LB film is and easier is its preparation. (iii) Insolubility of the dyad LB films in polar organic solvents would allow their application in photoelectrochemical experiments with the use of more efficient electron mediating species. (iv) Moreover, the herein developed film preparation procedure may allow for formation of photoelectrodes working as either a photoanode or photocathode depending on the employed mediators. However, the photoelectrode described in the present work preferentially operated as the photoanode. Most likely, this operation resulted from insufficient polarity of the phthalocyanine peripheral aliphatic ether chains, preventing from formation of the dyad LB films on hydrophilic substrates. Consequently, stable dyad LB films were formed on hydrophobic substrates and the resulting enforced dyad orientation allowed for the electron flow from the solution to the photoelectrode. Formation of the dyad readily transferrable on both the hydrophobic and hydrophilic substrate would lead to controllable formation of the photoelectrode operating as either the photoanode or photocathode equally well.

ASSOCIATED CONTENT

Supporting Information

Synthesis of tetrakis[2,9,16,23-tri(ethylene glycolmonomethyl ether) phthalocyaninato] Zn(II), Zn(TPPE), TOF MS ES+ spectra for Zn(TPPE), the UV–vis spectra for titration of Zn(TPPE), the surface pressure vs time dependence for the Zn(TPPE)-C_{60}im dyad Langmuir film, the LB transfer ratio for the Zn(TPPE)-C_{60}im dyad Langmuir film, AFM image of the Zn(TPPE)-C_{60}im dyad multilayer LB film on the Au-over-Ti coated glass slide, the DPV curves for the dyad and its components in a solution, consecutively recorded $I-V$ curves for the light-irradiated Zn(TPPE)-C_{60}im dyad multilayer LB film, the DFT/(B3LYP/3-21G*) optimized structure of HOMO and LUMO of the Zn(TPPE)-C_{60}im dyad, dipole moments of Zn(TPPE), C_{60}im and the Zn(TPPE)-C_{60}im dyad, schematic orientation of the dyad in the Langmuir film, possible orientation of the dyad LB film on a solid substrate, illustration of the mechanism of anodic photocurrent generation by the multilayer Langmuir–Blodgett film of the Zn(TPPE)-C_{60}im dyad, the acid–base and redox equilibria of L-ascorbic acid and methylviologen, the DFT estimated dipole moments and dipole moment components normal to the subphase for the dyad and its components separately. This material is available free of charge via Internet at http://pubs.acs.org.

AUTHOR INFORMATION

Corresponding Authors

*E-mail: wkutner@ichf.edu.pl. Fax: +48 22 343 33 33. Tel: +48 22 343 32 17.

*E-mail: francis.dsouza@unt.edu. Fax: +1 940-565-4318. Tel.: +1 940-369-8832.

Author Contributions

The manuscript was written through the contribution of all authors.

Funding

The present research was financially supported by the Polish National Science Centre (NCN, Grant 2011/01/N/ST5/05615 to I.O.), the European Regional Development Fund (ERDF, POIG.01.01.02−00−008/08 2007−2013) cofinanced from the European Regional Development Fund within the Innovative Economy Operational Programme "Grants for Innovations" to K.N. and W.K., the European Union 7.FP under Grant REGPOT-CT-2011−285949-NOBLESSE to K.N. and W.K., and the U.S. National Science Foundation (Grant CHE-1110942 to F.D.). The work of W.K. was partially accomplished within the International PhD Project Program of the Foundation for Polish Science (MPD/2009/1/styp15 and MPD/2009/1/styp19) financed by the European Regional Development Fund within the Innovative Economy Operational Program "Grants for Innovations." Access to the AFM instrumentation was granted due to funds from the Foundation for Polish Science under the FOCUS Programme 3/2010/ Grants to Dr. Joanna Niedziółka-Jönsson of IPC PAS.

Notes

The authors declare no competing financial interest.

ACKNOWLEDGMENTS

We thank Prof. Jacek Waluk for helpful discussion, Dr. Janusz W. Sobczak for the XPS measurements, as well as Prof. Jan Augustyński and Dr. Piotr Barczuk for help with photoelectrochemical experiments.

ABBREVIATIONS

Zn(TPPE), tetrakis(2,9,16,23-tri[ethylene glycolmonomethyl ether] phthalocyaninato)Zn(II),
C_{60}im, 2-(phenylimidazolyl)fullerenopyrrolidine.

REFERENCES

(1) Lewis, N. S.; Nocera, D. G. Powering the Planet: Chemical Challenges in Solar Energy Utilization. *Proc. Natl. Acad. Sci. U.S.A.* **2006**, *103*, 15729−15735.

(2) Turner, J. A. A Realizable Renewable Energy Future. *Science* **1999**, *285*, 687−689.

(3) Barber, J. Photosynthetic Energy Conversion: Natural and Artificial. *Chem. Soc. Rev.* **2009**, *38*, 185−196.

(4) Scholes, G. D.; Fleming, G. R.; Olaya-Castro, A.; van Grondelle, R. Lessons from Nature about Solar Light Harvesting. *Nat. Chem.* **2011**, *3*, 763−774.

(5) Concepcion, J. J.; House, R. L.; Papanikolas, J. M.; Meyer, T. J. Chemical Approaches to Artificial Photosynthesis. *Proc. Natl. Acad. Sci. U.S.A.* **2012**, *109*, 15560−15564.

(6) Kamat, P. V. Meeting the Clean Energy Demand: Nanostructure Architectures for Solar Energy Conversion. *J. Phys. Chem. C* **2007**, *111*, 2834−2860.

(7) Balzani, V.; Credi, A.; Venturi, M. Photochemical Conversion of Solar Energy. *ChemSusChem* **2008**, *1*, 26−58.

(8) Tkachenko, N. V.; Lemmetyinen, H. In *Handbook of Carbon Nano Materials*; D'Souza, F., Kadish, K. M., Eds.; World Scientific: Singapore, 2011; Vol. 2, pp 405−440.

(9) Lin, Y.; Li, Y.; Zhan, X. Small Molecule Semiconductors for High-Efficiency Organic Photovoltaics. *Chem. Soc. Rev.* **2012**, *41*, 4245−4272.

(10) Kippelen, B.; Bredas, J.-L. Organic Photovoltaics. *Energy Environ. Sci.* **2009**, *2*, 251−261.

(11) Walter, M. G.; Rudine, A. B.; Wamser, C. C. Porphyrins and Phthalocyanines in Solar Photovoltaic Cells. *J. Porphyrins Phthalocyanines* **2010**, *14*, 759−792.

(12) Martinez-Diaz, M. V.; de la Torre, G.; Torres, T. Lighting Porphyrins and Phthalocyanines for Molecular Photovoltaics. *Chem. Commun.* **2010**, *46*, 7090−7108.

(13) D'Souza, F.; Ito, O. Photosensitized Electron Transfer Processes of Nanocarbons Applicable to Solar Cells. *Chem. Soc. Rev.* **2012**, *41*, 86−96.

(14) Bikram, C. K. C.; Subbaiyan, N. K.; D'Souza, F. Supramolecular Donor-Acceptor Assembly Derived from Tetracarbazole-Zinc Phthalocyanine Coordinated to Fullerene: Design, Synthesis, Photochemical, and Photoelectrochemical Studies. *J. Phys. Chem. C* **2012**, *116*, 11964−11972.

(15) El-Khouly, M. E.; Ju, D. K.; Kay, K.-Y.; D'Souza, F.; Fukuzumi, S. Supramolecular Tetrad of Subphthalocyanine-Triphenylamine-Zinc Porphyrin Coordinated to Fullerene as an "Antenna-Reaction-Center" Mimic: Formation of a Long-Lived Charge-Separated State in Nonpolar Solvent. *Chem.—Eur. J.* **2010**, *16*, 6193−6202.

(16) Green, B. R.; Parson, W. W., Eds.; *Light-Harvsting Antennas in Photosynthesis*; Kluwer: Dordrecht, The Netherlands, 2003.

(17) Gust, D.; Moore, T. A.; Moore, A. L. Solar Fuels via Artificial Photosynthesis. *Acc. Chem. Res.* **2009**, *42*, 1890−1898.

(18) Bottari, G.; de la Torre, G.; Guldi, D. M.; Torres, T. Covalent and Noncovalent Phthalocyanine-Carbon Nanostructure Systems: Synthesis, Photoinduced Electron Transfer, and Application to Molecular Photovoltaics. *Chem. Rev.* **2010**, *110*, 6768−6816.

(19) Ince, M.; Hausmann, A.; Martinez-Diaz, M. V.; Guldi, D. M.; Torres, T. Non-Covalent Versus Covalent Donor-Acceptor Systems Based on Near-Infrared Absorbing Azulenocyanines and C_{60} Fullerene Derivatives. *Chem. Commun.* **2012**, *48*, 4058−4060.

(20) Wasielewski, M. R. Self-Assembly Strategies for Integrating Light Harvesting and Charge Separation in Artificial Photosynthetic Systems. *Acc. Chem. Res.* **2009**, *42*, 1910−1921.

(21) Osuka, A.; Mataga, N.; Okada, T. A Chemical Approach Towards the Photosynthetic Reaction Centre. *Pure Appl. Chem.* **1997**, *69*, 797−802.

(22) Fukuzumi, S.; Ohkubo, K.; D'Souza, F.; Sessler, J. L. Supramolecular Electron Transfer by Anion Binding. *Chem. Commun.* **2012**, *48*, 9801−9815.

(23) Flamigni, L.; Barigelletti, F.; Armaroli, N.; Collin, J.-P.; Dixon, I. M.; Sauvage, J.-P.; Williams, J. A. G. Photoinduced Processes in Multicomponent Arrays Containing Transition Metal Complexes. *Coord. Chem. Rev.* **1999**, *190−192*, 671−682.

(24) Imahori, H.; Umeyama, T.; Kurotobi, K.; Takano, Y. Self-Assembling Porphyrins and Phthalocyanines for Photoinduced Charge Separation and Charge Transport. *Chem. Commun.* **2012**, *48*, 4032−4045.

(25) Schuster, D. I.; Li, K.; Guldi, D. M. Porphyrin-Fullerene Photosynthetic Model Systems with Rotaxane and Catenane Architectures. *C. R. Chimie* **2006**, *9*, 892−908.

(26) D'Souza, F.; Ito, O. Recent Advances in Photoinduced Electron Transfer Processes of Fullerene-Based Molecular Assemblies and Nanocomposites. *Molecules* **2012**, *17*, 5816−5835.

(27) Li, H.; Babu, S. S.; Nakanishi, T. In *Supramolecular Chemistry of Fullerenes and Carbon Nanotubes*; Martin, N., Nierengarten, J. F., Eds.; Wiley-VCH Verlag & Co. KGaA: Weinheim, Germany, 2012; pp 127−158.

(28) Boyd, P. D. W.; Reed, C. A. Fullerene-Porphyrin Constructs. *Acc. Chem. Res.* **2004**, *38*, 235−242.

(29) Hasobe, T. Supramolecular Nanoarchitectures for Light Energy Conversion. *Phys. Chem. Chem. Phys.* **2010**, *12*, 44−57.
(30) D'Souza, F.; Ito, O. Photoinduced Electron Transfer in Supramolecular Systems of Fullerenes Functionalized with Ligands Capable of Binding to Zinc Porphyrins and Zinc Phthalocyanines. *Coord. Chem. Rev.* **2005**, *249*, 1410−1422.
(31) El-Khouly, M. E.; Ito, O.; Smith, P. M.; D'Souza, F. Intermolecular and Supramolecular Photoinduced Electron Transfer Processes of Fullerene-Porphyrin/Phthalocyanine Systems. *J. Photochem. Photobiol. C* **2004**, *5*, 79−104.
(32) Fukuzumi, S. Development of Bioinspired Artificial Photosynthetic Systems. *Phys. Chem. Chem. Phys.* **2008**, *10*, 2283−2297.
(33) El-Khouly, M. E.; Fukuzumi, S.; D'Souza, F. Photosynthetic Antenna-Reaction Center Mimicry by Using Boron Dipyrromethene Sensitizers. *ChemPhysChem* **2014**, *15*, 30−47.
(34) Yang, S.; Fan, L.; Yang, S. Preparation, Characterization, and Photoelectrochemistry of Langmuir-Blodgett Films of the Endohedral Metallofullerene Dy@C82 Mixed with Metallophthalocyanines. *J. Phys. Chem. B* **2003**, *107*, 8403−8411.
(35) Kaunisto, K.; Vahasalo, H.; Chukharev, V.; Tkachenko, N. V.; Vivo, P.; Niemi, M.; Tolkki, A.; Efimov, A.; Lemmetyinen, H. Photoinduced charge transfer through films containing poly(hexylthiophene), phthalocyanine, and porphyrin-fullerene layers. *Thin Solid Films* **2009**, *517*, 2988−2993.
(36) Tolkki, A.; Kaunisto, K.; Efimov, A.; Kivistoe, H.; Storbacka, L.; Savikoski, R.; Huttunen, K.; Lehtimaeki, S.; Lemmetyinen, H. Directed Electron Transfer in Langmuir-Schäfer Layers of Porphyrin-Fullerene and Phthalocyanine-Fullerene Dyads in Inverted Organic Solar Cells. *Phys. Chem. Chem. Phys.* **2012**, *14*, 3498−3504.
(37) Ranta, J.; Kaunisto, K.; Niskanen, M.; Efimov, A.; Hukka, T. I.; Lemmetyinen, H. Monoisomeric Phthalocyanines and Phthalocyanine-Fullerene Dyads with Polar Side Chains: Synthesis, Modeling, and Photovoltage. *J. Phys. Chem. C* **2014**, *118*, 2754−2765.
(38) Ulmann, P. A.; Tanaka, H.; Matsuo, Y.; Xiao, Z.; Soga, I.; Nakamura, E. Electric field dependent photocurrent generation in a thin-film organic photovoltaic device with a [70]fullerene-benzodifuranone dyad. *Phys. Chem. Chem. Phys.* **2011**, *13*, 21045−21049.
(39) Marczak, R.; Noworyta, K.; Nowakowski, R.; Kutner, W.; Desbat, B.; Araki, Y.; Ito, O.; Gadde, S.; Zandler, M. E.; D'Souza, F. Self Assembling of Porphyrin-Fullerene Dyads in the Langmuir and Langmuir-Blodgett Films: Formation as well as Spectral, Electrochemical and Vectorial Electron Transfer Studies. *J. Nanosci. Nanotechnol.* **2007**, *7*, 1455−1471.
(40) Marczak, R.; Sgobba, V.; Kutner, W.; Gadde, S.; D'Souza, F.; Guldi, D. M. Langmuir-Blodgett Films of a Cationic Zinc Porphyrin-Imidazole-Functionalized Fullerene Dyad: Formation and Photoelectrochemical Studies. *Langmuir* **2007**, *23*, 1917−1923.
(41) Subbaiyan, N. K.; Obraztsov, I.; Wijesinghe, C. A.; Tran, K.; Kutner, W.; D'Souza, F. Supramolecular Donor-Acceptor Hybrid of Electropolymerized Zinc Porphyrin with Axially Coordinated Fullerene: Formation, Characterization, and Photoelectrochemical Properties. *J. Phys. Chem. C* **2009**, *113*, 8982−8989.
(42) D'Souza, F.; Deviprasad, G. R.; Zandler, M. E.; Hoang, V. T.; Klykov, A.; Van Stipdonk, M.; Perera, A.; El-Khouly, M. E.; Fujitsuka, M.; Ito, O. Spectroscopic, Electrochemical, and Photochemical Studies of Self-Assembled via Axial Coordination Zinc Porphyrin−Fulleropyrrolidine Dyads. *J. Phys. Chem. A* **2002**, *106*, 3243−3252.
(43) Frisch, M. J.; Trucks, G. W.; Schlegel, H. B.; Scuseria, G. E.; Robb, M. A.; Cheeseman, J. R.; Scalman, G.; Barone, V.; Mennucci, B.; Petersson, G. A.; Nakatsuji, H.; Caricato, M.; Li, X.; Hratchian, H. P.; Izmaylov, A. F.; Bloino, J.; Zheng, G.; Sonnenberg, J. L.; Hada, M.; Ehara, M.; Toyota, K.; Fukuda, R.; Hasegawa, J.; Ishida, M.; Nakajima, T.; Honda, Y.; Kitao, O.; Nakai, H.; Vreven, T.; Montgomery, J. A.; Peralta, J. E.; Ogliaro, F.; Bearpark, M.; Heyd, J. J.; Brothers, E.; Kudin, K. N.; Staroverov, V. N.; Kobayashi, R.; Normand, J.; Raghavachari, K.; Rendell, A.; Burant, J. C.; Iyengar, S. S.; Tomasi, J.; Cossi, M.; Rega, N.; Millam, J. M.; Klene, M.; Knox, J. E.; Cross, J. B.; Bakken, V.; Adamo, C.; Jaramillo, J.; Gomperts, R.; Stratmann, R. E.; Yazyev, O.; Austin, A. J.; Cammi, R.; Pomelli, C.; Ochterski, J. W.; Martin, R. L.; Morokuma, K.; Zakrzewski, V. G.; Voth, G. A.; Salvador, P.; Dannenberg, J. J.; Dapprich, S.; Daniels, A. D.; Farkas, Ö.; Foresman, J. B.; Ortiz, J. V.; Cioslowski, J.; Fox, D. J. *Gaussian 09*; Gaussian, Inc.: Wallingford, CT, 2009.
(44) D'Souza, F.; Rath, N. P.; Deviprasad, G. R.; Zandler, M. E. Structural Studies of a Noncovalently Linked Porphyrin-Fullerene Dyad. *Chem. Commun.* **2001**, 267−268.
(45) El-Khouly, M. E.; Rogers, L. M.; Zandler, M. E.; Gadde, S.; Fujitsuka, M.; Ito, O.; D'Souza, F. Studies on Intra-Supramolecular and Intermolecular Electron-Transfer Processes between Zinc Naphthalocyanine and Imidazole-Appended Fullerene. *ChemPhysChem* **2003**, *4*, 474−481.
(46) KC, C. B.; Stranius, K.; D'Souza, P.; Subbaiyan, N. K.; Lemmetyinen, H.; Tkachenko, N. V.; D'Souza, F. Sequential Photoinduced Energy and Electron Transfer Directed Improved Performance of the Supramolecular Solar Cell of a Zinc Porphyrin-Zinc Phthalocyanine Conjugate Modified TiO_2 Surface. *J. Phys. Chem. C* **2013**, *117*, 763−773.
(47) Davies, J. T.; Rideal, E. K. In *Interfacial Phenomena*; Academic Press: London, 1961; pp 217−281.
(48) Zeyada, H. M.; El-Nahass, M. M. Electrical Properties and Dielectric Relaxation of Thermally Evaporated Zinc Phthalocyanine Thin Films. *Appl. Surf. Sci.* **2008**, *254*, 1852−1858.
(49) Smallwood, I. M. *Handbook of Organic Solvent Properties*; John Wiley & Sons: London, 1996.
(50) Chern, G.; Mathias, H.; Testardi, L. R.; Seger, L.; Schlenoff, J. Low-Frequency Dielectric Permittivity of C_{60}. *J. Supercond.* **1995**, *8*, 207−210.
(51) Davies, J. T.; Rideal, E. K. In *Interfacial Phenomena*; Academic Press: London, 1961; pp 265.
(52) Bethencourt, M. I.; Srisombat, L.; Chinwangso, P.; Lee, T. R. SAMs on Gold Derived from the Direct Adsorption of Alkanethioacetates Are Inferior to Those Derived from the Direct Adsorption of Alkanethiols. *Langmuir* **2009**, *25*, 1265−1271.
(53) Leitch, J.; Kunze, J.; Goddard, J. D.; Schwan, A. L.; Faragher, R. J.; Naumann, R.; Knoll, W.; Dutcher, J. R.; Lipkowski, J. In Situ PM-IRRAS Studies of an Archaea Analogue Thiolipid Assembled on a Au(111) Electrode Surface. *Langmuir* **2009**, *25*, 10354−10363.
(54) Jiang, J.; Bao, M.; Rintoul, L.; Arnold, D. P. Vibrational Spectroscopy of Phthalocyanine and Naphthalocyanine in Sandwich-Type (na)Phthalocyaninato and Porphyrinato Rare Earth Complexes. *Coord. Chem. Rev.* **2006**, *250*, 424−448.
(55) Brosseau, C. L.; Leitch, J.; Bin, X.; Chen, M.; Roscoe, S. G.; Lipkowski, J. Electrochemical and PM-IRRAS a Glycolipid-Containing Biomimetic Membrane Prepared Using Langmuir-Blodgett/Langmuir-Schaefer Deposition. *Langmuir* **2008**, *24*, 13058−13067.
(56) Pereira, A. M. V. M; Hausmann, A.; Tome, J. P. C.; Trukhina, O.; Urbani, M.; Neves, M. G. P. M. S.; Cavaleiro, J. A. S.; Guldi, D. M.; Torres, T. Porphyrin-Phthalocyanine/Pyridylfullerene Supramolecular Assemblies. *Chem.—Eur. J.* **2012**, *18*, 3210−3219.
(57) Das, S. K.; Mahler, A.; Wilson, A. K.; D'Souza, F. High Potential Perfluorinated Phthalocyanine-Fullerene Dyads for Generation of High Energy Charge Separated States: Formation and Photoinduced Electron Transfer Studies. *ChemPhysChem* **2014**, DOI: 10.1002/cphc.201402118.
(58) D'Souza, F.; Ito, O. Light Induced Electron Transfer Processes of Functionalized Nanocarbons: Fullerenes, Nanotubes and Graphene. *Sci. Prog.* **2013**, *96*, 369−397.
(59) Mortimer, R. J. Electrochromic materials. *Chem. Soc. Rev.* **1997**, *26*, 147−156.
(60) Njus, D.; Jalukar, V.; Zu, J. A.; Kelley, P. M. Concerted Proton-Electron Transfer Between Ascorbic Acid and Cytochrome b561. *Am. J. Clin. Nutr.* **1991**, *54*, 1179S−1183S.